## Electronic Supplementary Information

# $NH_4V_3O_8 \cdot 0.5H_2O$ Nanobelts with Intercalated Water Molecules as High Performance Zinc Ion Battery Cathode

Hanmei Jiang[1], Yifu Zhang[*,1,2], Zhenghui Pan[*,2], Lei Xu[1], Jiqi Zheng[1], Zhanming Gao[1], Tao Hu[1], Changgong Meng[1], John Wang[*,2]

[1]*School of Chemical Engineering, Dalian University of Technology, Dalian 116024, PR China*

[2]*Department of Materials Science and Engineering, National University of Singapore, 117574 Singapore, Singapore*

*E-mail addresses: yfzhang@dlut.edu.cn (Y. Zhang), msepz@nus.edu.sg (Z. Pan); msewangj@nus.edu.sg (J. Wang)

## Experimental section

### *Synthesis of $NH_4V_3O_8·0.5H_2O$ nanowires*

All chemicals purchased from Sinopharm Chemical Reagent Co., Ltd were with analytical grade and used without any further purification. In a typical procedure, 0.585 g of $NH_4VO_3$, 0.63 g of $H_2C_2O_4·2H_2O$ and 35 mL distilled water were mixed and magnetic stirred for 30 min at the room temperature. The above solution was transferred into a 50 mL Teflon-lined stainless steel autoclave and kept at 110 °C for 8 h. After the reaction, the products were filtered off, washed with distilled $H_2O$ and absolute ethanol several times to remove any possible residues, and dried in vacuum at 75 °C over night to obtain $NH_4V_3O_8·0.5H_2O$ nanowires.

### *Materials characterization*

The phase and composition of the products were identified by X-ray powder diffraction (XRD, Panalytical X'Pert powder diffractometer at 40 kV and 40 mA with Ni-filtered Cu Kα radiation). The chemical composition of as-obtained samples was revealed by use of an energy-dispersive X-ray spectrometer (EDS) and EDS mapping attached to a scanning electron microscope (SEM, QUANTA450). X-ray photoelectron spectroscopy (XPS) was used to investigate the composition of the products and confirm the oxidation state of vanadium performed on ESCALAB250Xi, Thermo Fisher Scientific. The Raman spectra were obtained using a Thermo Scientific spectrometer, with a 532 nm excitation line. Fourier transform infrared spectroscopy (FTIR) pattern of the solid samples was measured using KBr pellet technique (About 1 wt. % of the samples and 99 wt. % of KBr were mixed homogeneously, and then the mixture was pressed to a pellet) and recorded on a Nicolet 6700 spectrometer from 4000 to 400 $cm^{-1}$ with a resolution of 4 $cm^{-1}$. The morphology and dimensions of the products were observed by field emission scanning electron microscopy (FE-SEM, NOVA NanoSEM 450, FEI) and transmission electron microscopy (TEM, FEITecnai F30, FEI). The high-resolution transmission electron microscopy (HRTEM) and selected area electron diffraction (SAED) were also carried out on FEITecnai F30. The samples were dispersed in absolute ethanol with ultrasonication before TEM characterization.

For the ex situ XRD, Raman and XPS characterizations, the cycled electrodes were washed with deionized water and dried naturally in air. But as for the ex situ TEM investigations, the cycled electrodes could easily peel off from the titanium foil and then ultrasound with alcohol.

***Electrochemical characterization***

Electrochemical tests of the $NH_4V_3O_8 \cdot 0.5H_2O$ nanowires were performed with CR2032 coin-type cells. The working electrode was fabricated by mixing the active material, a conductive agent (Super-P, Sigma-Aldrich), and PVDF (Sigma-Aldrich), in a weight ratio of 7 : 2 : 1. Next, the mixture was coated on Ti sheet. The total mass of the electrode materials was around 2 mg, measured by an ultramicro analytical balance (Mettler Toledo XP2U, 0.1 mg resolution). After drying in air at 90 °C for 12 h, the electrodes were assembled in coin type cells (CR2032) and zinc foil and glass fiber (Whatman GF/A) were employed as the anode and separator, respectively. A 3 M $Zn(CF_3SO_3)_2$ aqueous solution was used as the electrolyte. Cyclic voltammetry (0.3–1.3 V) and electrochemical impedance spectroscopy (EIS) were performed on a CHI 660D electrochemical workstation. The charge/discharge tests were performed using a Wuhan LAND battery tester at different current rates.

**Figure S1**

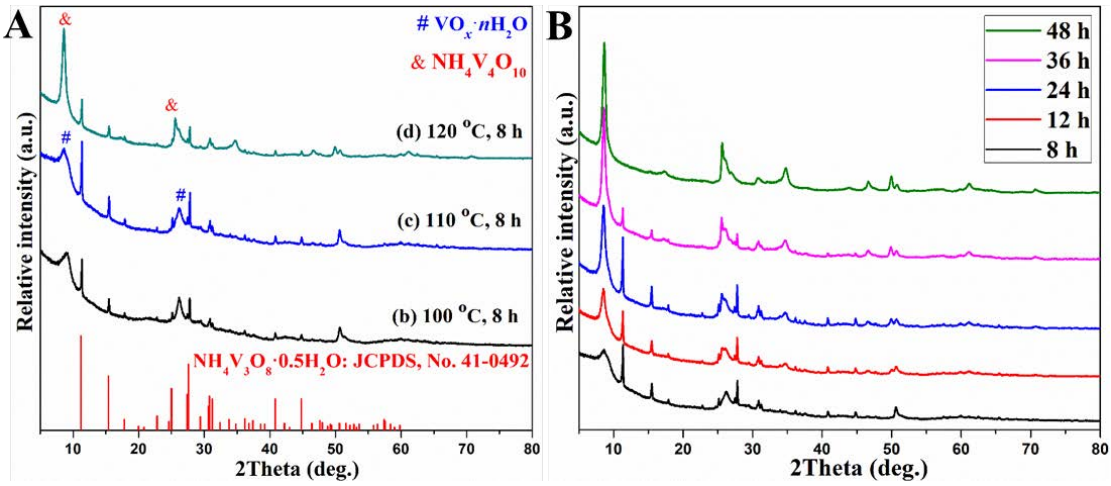


Figure S1. XRD patterns of the samples synthesized with different conditions: (A) at various reaction temperatures for 8 h; (B) at 110 °C for various reaction times.

$NH_4V_3O_8 \cdot 0.5H_2O$ nanowires were synthesized using $NH_4VO_3$ and $H_2C_2O_4 \cdot 2H_2O$ as the starting materials by a facile hydrothermal method and this route is convenience and large-scale. Figure S1A shows the XRD patterns of the samples obtained at different reaction temperatures for 8 h. When the reaction temperature is at 100 °C, the mixture of $NH_4V_3O_8 \cdot 0.5H_2O$ and $VO_x \cdot nH_2O$ are obtained. With the reaction temperature increasing, the phase of $VO_x \cdot nH_2O$ decreases and it converts to $NH_4V_4O_{10}$. At 110 °C, the dominated phase is $NH_4V_3O_8 \cdot 0.5H_2O$ with minor $VO_x \cdot nH_2O$. However, the phase is major $NH_4V_4O_{10}$ with minor $NH_4V_3O_8 \cdot 0.5H_2O$. Figure S1B shows the XRD patterns of the samples obtained at 110 °C for different reaction times. With the reaction time increasing, the phase gradually changes to $NH_4V_4O_{10}$, and the phase is complete $NH_4V_4O_{10}$ at 110 °C for 48 h. Figures S2 show the FE-SEM images of the samples obtained at various reaction conditions. The wire-like morphology is obtained at 100 °C for 8 h (Figure S2a), however the shape changes to sheet-like morphology at 120 °C for 8 h (Figure S2b). With the increase of the reaction time, the wire-like morphology changes to sheet-like morphology (Figures 1c and S2c-d). Thus, the optimized parameter of the preparation of $NH_4V_3O_8 \cdot 0.5H_2O$ is at 110 °C for 8 h, although it contains minor $VO_x \cdot nH_2O$.

**Figure S2**

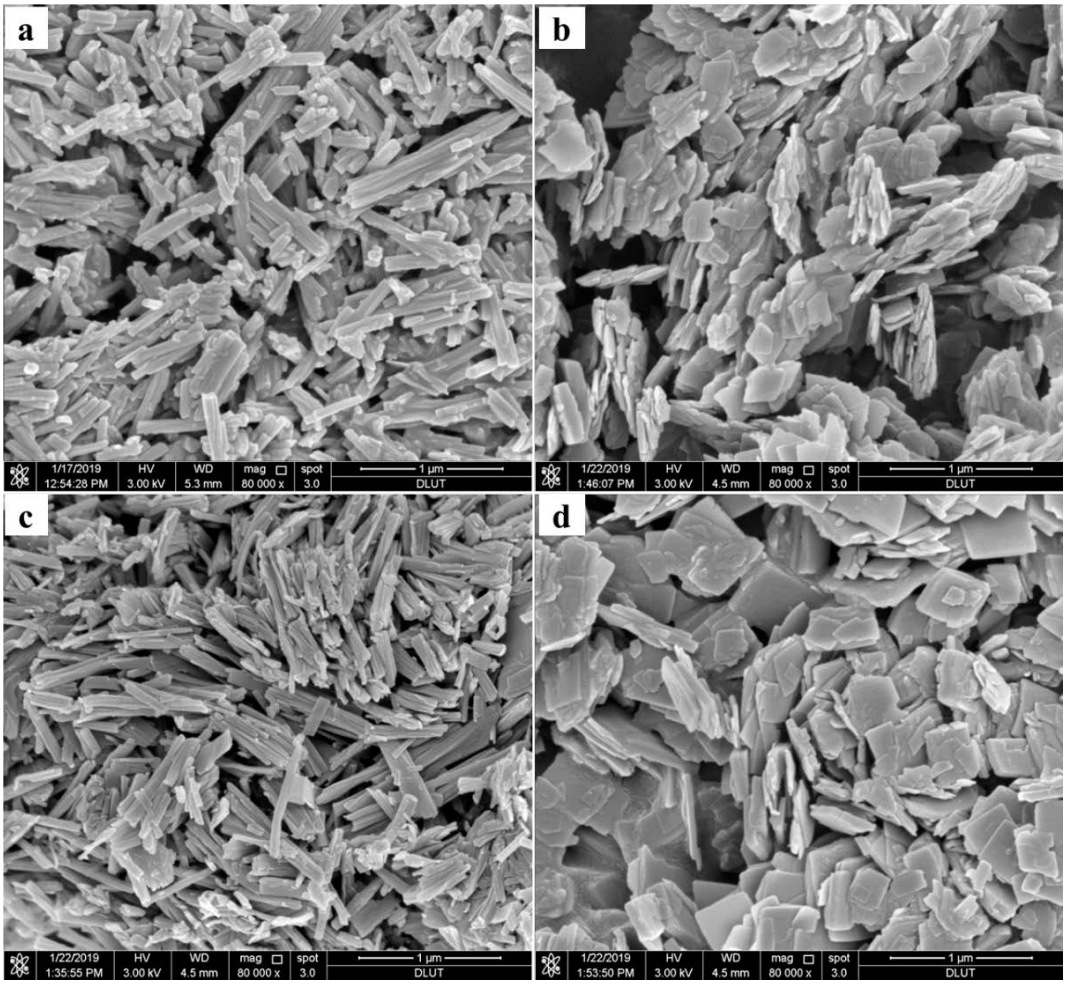


Figure S2. FE-SEM images of the samples synthesized with different conditions: (a) at 100 °C for 8 h; (b) at 120 °C for 8 h; (c) at 110 °C for 12 h; (c) at 110 °C for 36 h.

**Figure S3**

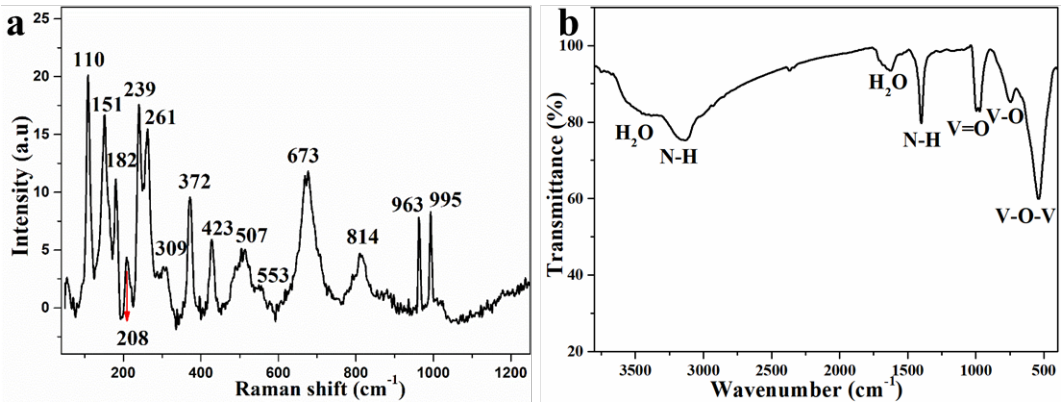


Figure S3. Raman (a) and FTIR (b) spectra of $NH_4V_3O_8 \cdot 0.5H_2O$ nanowires.

**Figure S4**

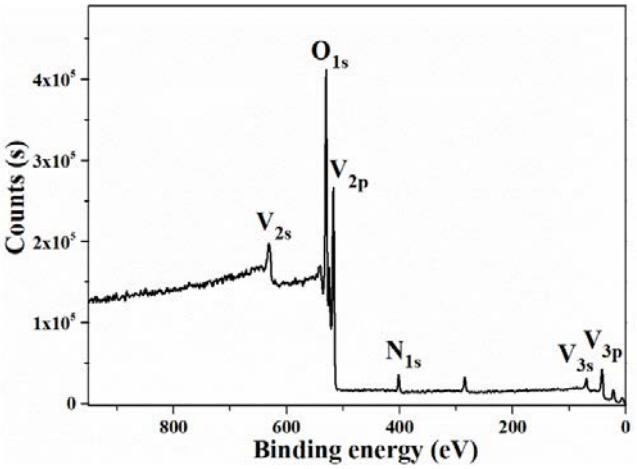


Figure S4. XPS full spectrum of $NH_4V_3O_8 \cdot 0.5H_2O$ nanowires.

**Figure S5**

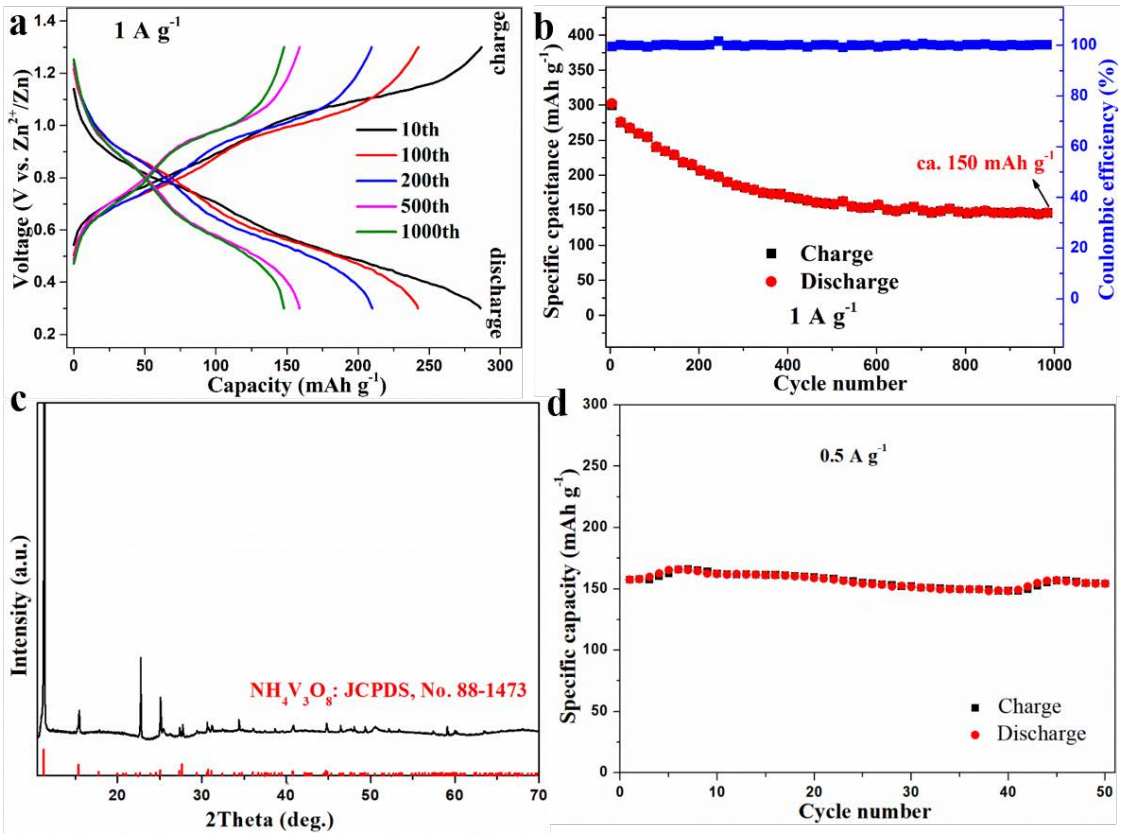


Figure S5. (a-b) Cycling performance at 1 $A \cdot g^{-1}$ of $Zn//NH_4V_3O_8 \cdot 0.5H_2O$ battery; Characterizations of $NH_4V_3O_8$ (c) XRD patterns; (d) Cycling performance at 0.5 $A \cdot g^{-1}$ of $Zn//NH_4V_3O_8$ battery.

$NH_4V_3O_8$ was prepared by modified reported method[1]. 0.585 g $NH_4V_3O_8$ was dissolved in 80 mL deionized water to form a light-yellow solution at 80°C, then an appropriate amount of dilute hydrochloric acid (1 M) was added dropwise under continuous stirring to adjust the desired pH value of the solution to about 2.0. Then, the resulting solution was maintained at 90°C for 2.5h with water-bath and then allowed to cool down to room temperature naturally. The product was washed several times with deionized water, and then dried at 60 °C in oven for 12h to obtain $NH_4V_3O_8$, as shown in Figure S5c.

**Figure S6**

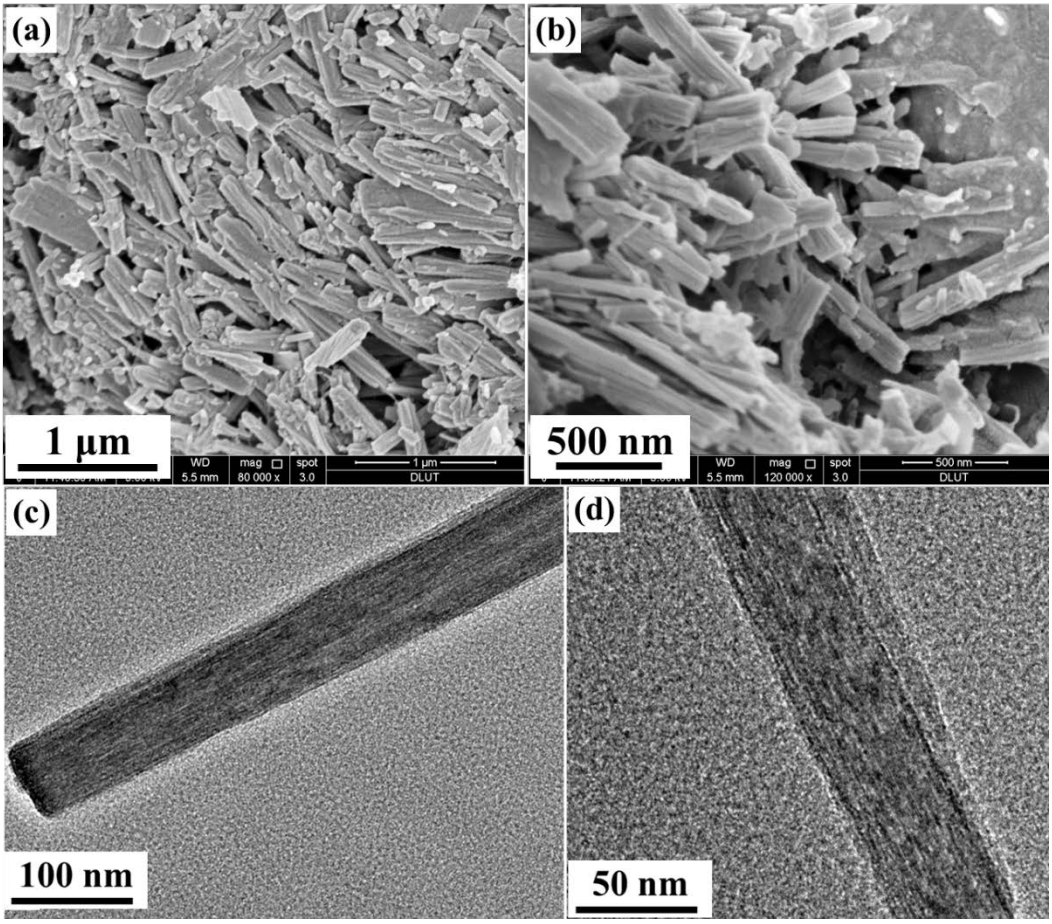


**Figure S6.** FE-SEM (a, b) and TEM (c, d) images of the cathode materials in Zn//$NH_4V_3O_8 \cdot 0.5H_2O$ battery after cycles.

**Figure S7**

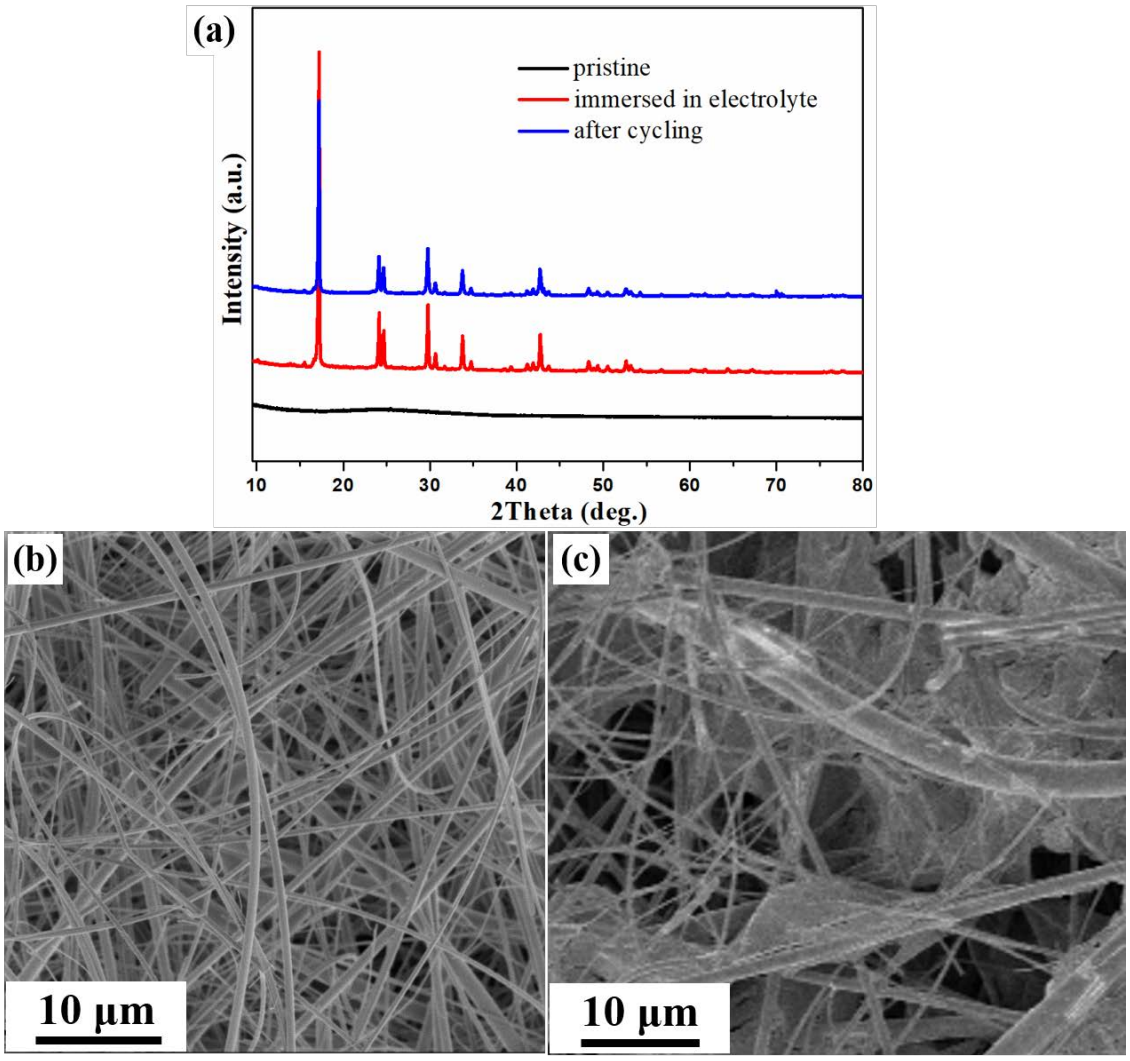


**Figure S7. (a) XRD of glass fiber; (b) SEM of pristine glass fiber; (c) SEM of glass fiber after 1000 cycles at 1 $A \cdot g^{-1}$ in Zn//$NH_4V_3O_8 \cdot 0.5H_2O$ battery.**

**Figure S8**

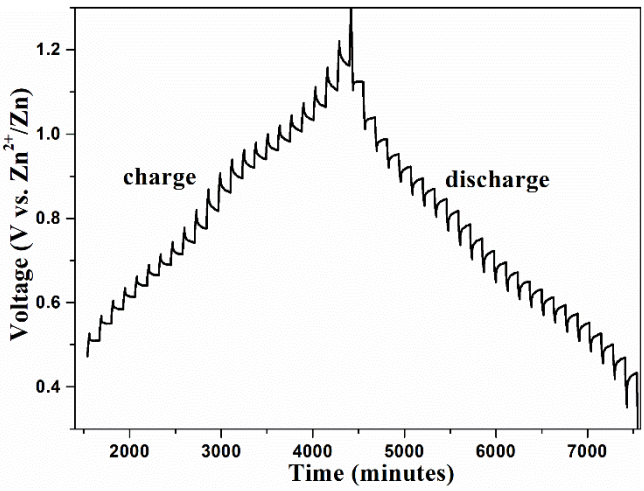


**Figure S8.** GITT curves: the voltage vs. the discharge/charge time.

Before the GITT measurement, the assembled cell was first discharged/charged at 100 mA $g^{-1}$ for 6 cycles to obtain a stable state. Subsequently, the cell was discharged or charged at 100 mA $g^{-1}$ for 20 min, and then relaxed for 120 min to make the voltage reach the equilibrium. The procedure was repeatedly applied to the cell during the entire charge/discharge process. The $Zn^{2+}$ diffusion coefficient can be calculated based on the following equation [2, 3]:

$$D_{Zn^{2+}} = \frac{4}{\pi\tau}\left(\frac{m_B V_M}{M_B S}\right)^2 \left(\frac{\Delta E_S}{\Delta E_\tau}\right)^2$$

where $\tau$ is the duration time of the current pulse, $m_B$ is the mass of the active material, $M_B$ is the molecular weight (g/mol) and $V_M$ is its molar volume ($cm^3$/mol), S is the total contacting area of electrode with electrolyte, $\Delta E_S$ and $\Delta E_\tau$ are the change in the steady state voltage and overall cell voltage after the application of a current pulse in a single step GITT experiment, respectively.

**$Zn^{2+}$ diffusion coefficient from EIS**

The $Zn^{2+}$ diffusion coefficients of $Zn//NH_4V_3O_8{\cdot}0.5H_2O$ battery at various cycles are calculated using EIS by the following equation:

$$D_{Zn^{2+}}^{EIS} = \frac{R^2T^2}{2A^2n^4F^4C^2\sigma_w^2}$$

where R (8.314 J $mol^{-1}$ $K^{-1}$) is the gas constant, T (298 K) is the absolute temperature, F (96500 C $mol^{-1}$) is the Faraday constant, A ($cm^2$), C (mol $cm^{-3}$) and n are the surface area of the electrode, concentration of ion in the electrolyte and number of electrons transferred per molecule, respectively. Warburg coefficient ($\sigma_w$) is the slope of $Z'-\omega^{-1/2}$ at low frequency area, $\omega$ (Rad $s^{-1}$) is the angular frequency.

**Figure S9**

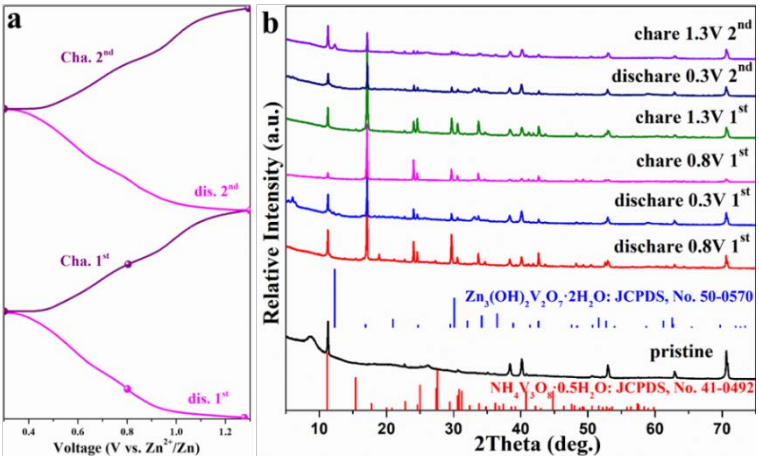


**Figure S9.** The discharge/charge states (a) and e*x situ* XRD patterns of the material at different discharge/charge states (b) in Zn//$NH_4V_3O_8 \cdot 0.5H_2O$ battery.

**Figure S10**

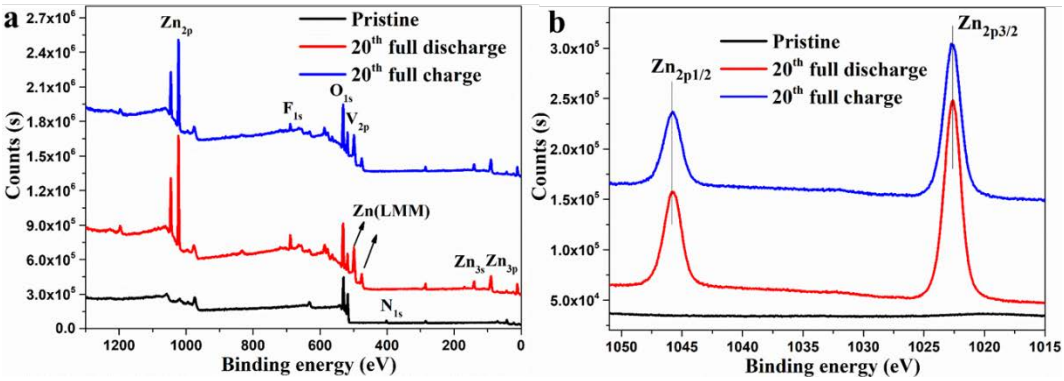


**Figure S10.** *Ex situ* full XPS spectra (a) and $Zn_{2p}$ core-level XPS spectra (b) of the cathode materials at different discharge/charge states in Zn//$NH_4V_3O_8 \cdot 0.5H_2O$ battery.

**Figure S11**

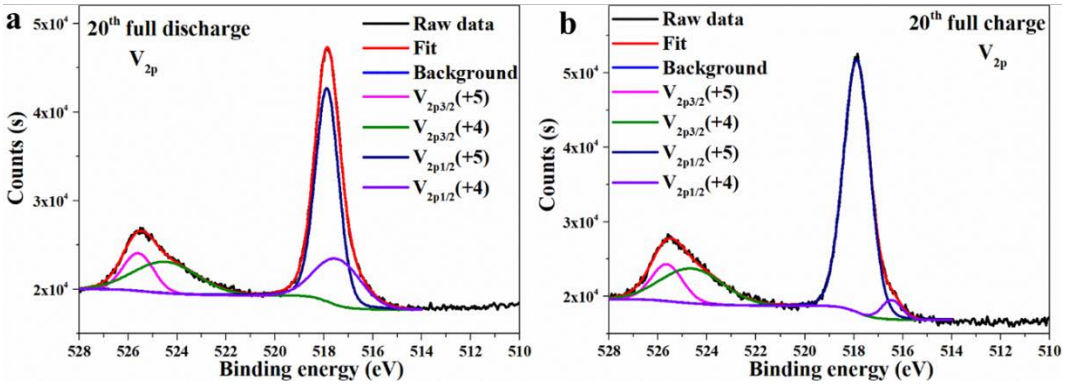


**Figure S11.** *Ex situ* $V_{2p}$ core-level XPS spectra of the cathode materials at different discharge/charge states in Zn//$NH_4V_3O_8 \cdot 0.5H_2O$ battery: (a) full discharge; (b) full charge.

**Table S1**

Table S1. Comparison of the electrochemical performance of **$NH_4V_3O_8·0.5H_2O$** with the state-of-the-art reported ammonium vanadates cathode materials.

| Cathode Materials | Capacity | Cycle performance | Ref. |
|---|---|---|---|
| **$NH_4V_3O_8·0.5H_2O$** | **423, 399, 380, 364, 344, 306 and 266 mA h $g^{-1}$ at 0.1, 0.2, 0.3, 0.4, 0.6, 0.8 and 1.0 A $g^{-1}$** | **400 mA h $g^{-1}$ at 0.1 A·$g^{-1}$ after 70 cycles<br>330 mA h $g^{-1}$ at 0.2 A·$g^{-1}$ after 120 cycles<br>148 mA h $g^{-1}$ at 1 A $g^{-1}$ after 1000 cycles** | **This work** |
| $NH_4V_3O_8$ | ~55 mAh $g^{-1}$ at 0.5 A $g^{-1}$ | ~60 mA h $g^{-1}$ at 0.1 A·$g^{-1}$ after 100 cycles | [4] |
| $(NH_4)_2V_3O_8$ | ~160 mAh $g^{-1}$ at 0.1 A $g^{-1}$ | ~75 mA h $g^{-1}$ at 0.1 A·$g^{-1}$ after 100 cycles | [4] |
| $NH_4V_4O_{10}$ | 380.3 mAh $g^{-1}$ at 0.1 A $g^{-1}$<br>361.6 mAh $g^{-1}$ at 1 A $g^{-1}$ | 125.6 mA h $g^{-1}$ at 0.1 A·$g^{-1}$ after 100 cycles<br>275.3 mA h $g^{-1}$ at 1 A·$g^{-1}$ after 100 cycles<br>255.5 mA h $g^{-1}$ at 10 A $g^{-1}$ after 1000 cycles | [4] |
| $NH_4V_4O_{10}$ nanobelt | 147, 126, 104, 91 and 72 mAh $g^{-1}$ at 0.05, 0.2, 0.6, 1.0 and 2.0 A $g^{-1}$, respectively. | ~90 mA h $g^{-1}$ at 0.5 A·$g^{-1}$ after 500 cycles<br>~70 mA h $g^{-1}$ at 1.0 A $g^{-1}$ after 1000 cycles | [5] |
| $(NH_4)_2V_{10}O_{25}·8H_2O$ | 228.8, 216.2, 196.1, 180.0, 156.7 and 123.6 mAh $g^{-1}$ at 0.1, 0.2, 0.5, 1.0, 2.0 and 5.0 A $g^{-1}$, respectively. | ~220 mA h $g^{-1}$ at 0.1 A·$g^{-1}$ after 100 cycles<br>~170 mA h $g^{-1}$ at 0.5 A $g^{-1}$ after 1000 cycles | [6] |
| $(NH_4)_2V_6O_{16}·1.5H_2O$ | 479.4, 399.6, 345.8, 295.3, and 215.1 mAh $g^{-1}$ at 0.1, 0.3, 0.5, 1, and 3 A $g^{-1}$, respectively. | 209.6 mA h $g^{-1}$ at 3 A·$g^{-1}$ after 1000 cycles | [7] |

**Table S2**

Table S2. Comparison of the cycle performance between the previous cathode materials for ARZIBs and this work.

| Cathode Materials | Electrochemical Performance (Capacity retention) | Ref. |
|---|---|---|
| **$NH_4V_3O_8·0.5H_2O$** | **400 mA h $g^{-1}$ at 0.1 A·$g^{-1}$ after 70 cycles<br>330 mA h $g^{-1}$ at 0.2 A·$g^{-1}$ after 120 cycles<br>148 mA h $g^{-1}$ at 1 A $g^{-1}$ after 1000 cycles** | **This work** |
| $LiV_3O_8$ | 172 mA h $g^{-1}$ at 0.133 A $g^{-1}$ after 65 cycles | [8] |
| $Fe_5V_{15}O_{39}(OH)_9·9H_2O$ | About 100 mA h $g^{-1}$ at 5 A $g^{-1}$ after 300 cycles | [9] |
| $V_2O_5$ | 110 mA h $g^{-1}$ at 2 A $g^{-1}$ after 2000 cycles | [10] |
| $VO_{1.52}(OH)_{0.77}$ | 105 mA h $g^{-1}$ at 0.015 A $g^{-1}$ after 50 cycles | [11] |
| $H_2V_3O_8$ | 136.1 mA h $g^{-1}$ at 5 A $g^{-1}$ after 1000 cycles | [12] |
| $V_2O_5·nH_2O$ | About 220 mA h $g^{-1}$ at 6 A $g^{-1}$ after 900 cycles | [13] |
| $K_2V_8O_{21}$ | 128.3 mA h $g^{-1}$ at 6 A $g^{-1}$ after 300 cycles | [14] |
| $Ag_{0.4}V_2O_5$ | 144 mA h $g^{-1}$ at 20 A $g^{-1}$ after 4000 cycles | [9] |
| $VS_2$ | 110.9 mA h $g^{-1}$ at 0.5 A $g^{-1}$ after 200 cycles | [15] |
| α−$Zn_2V_2O_7$ | 138 mA h $g^{-1}$ at 4 A $g^{-1}$ after 1000 cycles | [16] |
| $Zn_3V_2O_7(OH)_2·2H_2O$ | 101 mA h $g^{-1}$ at 0.2 A $g^{-1}$ after 300 cycles | [17] |
| $ZnMn_2O_4$ | 106.5 mA h $g^{-1}$ at 0.1 A $g^{-1}$ after 300 cycles | [18] |
| $Na_{1.1}V_3O_{7.9}$@rGO | 171 mA h $g^{-1}$ at 0.3 A $g^{-1}$ after 100 cycles | [19] |
| $MnO_2$ | 135 mA h $g^{-1}$ at 2 A $g^{-1}$ after 2000 cycles | [20] |
| β−$MnO_2$ | 135 mA h $g^{-1}$ at 0.2 A $g^{-1}$ after 200 cycles | [21] |
| α−$Mn_2O_3$ | 82.2 mA h $g^{-1}$ at 2 A $g^{-1}$ after 1000 cycles | [22] |
| $Mn_3O_4$ | 106.1 mA h $g^{-1}$ at 0.5 A $g^{-1}$ after 300 cycles | [23] |
| ZnHCF@$MnO_2$ | About 80 mA h $g^{-1}$ at 0.5 A $g^{-1}$ after 1000 cycles | [24] |
| $Na_3V_2(PO_4)_2F_3$ | 63.8 mA h $g^{-1}$ at 6 A $g^{-1}$ after 600 cycles | [25] |

**Table S3**

Table S3. Comparison of the electrochemical performance of **$NH_4V_3O_8 \cdot 0.5H_2O$** with the state-of-the-art reported cathode materials.

| Cathode Materials | Electrochemical Performance | Ref. |
|---|---|---|
| **$NH_4V_3O_8 \cdot 0.5H_2O$** | **423, 399, 380, 364, 344, 306 and 266 mA h $g^{-1}$ at 0.1, 0.2, 0.3, 0.4, 0.6, 0.8 and 1.0 A $g^{-1}$** | **This work** |
| $(NH_4)_2V_3O_8$ | ~160 mAh $g^{-1}$ at 0.1 A $g^{-1}$ | 4 |
| $NH_4V_4O_{10}$ | 361.6 mAh $g^{-1}$ at 1 A $g^{-1}$<br>380.3 mAh $g^{-1}$ at 0.1 A $g^{-1}$ | 4 |
| $NH_4V_3O_8$ | ~80 mAh $g^{-1}$ at 0.1 A $g^{-1}$ | 4 |
| $NH_4V_4O_{10}$ nanobelt | 147 mAh $g^{-1}$ at 0.05 A $g^{-1}$ | 5 |
| $Zn_{0.25}V_2O_5 \cdot nH_2O$ | 300, 260 and 223 mAh $g^{-1}$ at C/6, 1 C, and 15 C, respectively. (1C=300 mA $g^{-1}$) | 26 |
| $Mg_{0.34}V_2O_5 \cdot nH_2O$ | 353, 330, 291, 264 and 81 mAh $g^{-1}$ at 0.05, 0.1, 0.5, 1 and 5 A $g^{-1}$, respectively | 27 |
| $Ca_{0.25}V_2O_5 \cdot nH_2O$ | 340, and 289 mAh $g^{-1}$ at 0.2 C and 1C, respectively. (1C=250 mA $g^{-1}$) | 28 |
| $LiV_3O_8$ | 256, 311, 172, 148, and 47 mAh $g^{-1}$ at 0.016, 0.066, 0.133, 0.266 and 1.066 A $g^{-1}$, respectively. | 8 |
| $Na_{1.1}V_3O_{7.9}$ nanoribbons/graphene | 191 mAh $g^{-1}$ at 0.05 A $g^{-1}$ | 19 |
| $Na_{0.33}V_2O_5$ nanowire | 367.1, 253.7, 173.4, 137.5 and 96.4 mAh $g^{-1}$ at 0.1, 0.2, 0.5, 1, and 2 A $g^{-1}$, respectively. | 29 |
| $Na_5V_{12}O_{32}$ ($Na_{1.25}V_3O_8$) | 281 mAh $g^{-1}$ at 0.5 A $g^{-1}$ | 30 |
| $HNaV_6O_{16} \cdot 4H_2O$ ($H_{0.5}Na_{0.5}V_3O_8 \cdot 2H_2O$) | 304 mAh $g^{-1}$ at 0.5 A $g^{-1}$ | 30 |
| β-$Na_{0.33}V_2O_5$-type tunneled structure $Na_{0.76}V_6O_{15}$ ($Na_{0.253}V_2O_5$) | 135 mAh $g^{-1}$ at 0.5 A $g^{-1}$ | 30 |
| $Na_2V_6O_{16} \cdot 1.63H_2O$ nanowire | 352, 261, and 219 mAh $g^{-1}$ at 0.05, 0.5 and 1 A $g^{-1}$, respectively | 31 |
| $Zn_3V_2O_7(OH)_2 \cdot 2H_2O$ | 200, 122, 84 and 54 mAh $g^{-1}$ at 0.05, 0.5, 1 and 3 A $g^{-1}$, respectively | 17 |
| $Zn_2(OH)VO_4$ | 204, 160 and 101 mAh $g^{-1}$ at 0.5 C, 10 C and 50 C, respectively. (1 C= 200 mA $g^{-1}$) | 24 |
| $Fe_5V_{15}O_{39}(OH)_9 \cdot 9H_2O$ | 385 mAh $g^{-1}$ at 0.1A $g^{-1}$ | 9 |
| a-$Zn_2V_2O_7$ | 248, 231, 223, 218, 213, 209, 205, 190, and 170 mAh $g^{-1}$ at 50, 100, 200, 300, 500, 700, 900,1100, 2200, and 4400 mA $g^{-1}$, respectively. | 16 |
| $VO_2$(B) nanofibers | 357 mAh $g^{-1}$ at 0.1 A $g^{-1}$ | 32 |
| $VO_2$(B)/rGO | 365 mAh $g^{-1}$ at 0.05 A $g^{-1}$ | 33 |
| $VO_2$(B) | 338 mAh $g^{-1}$ at 0.05 A $g^{-1}$ | 33 |

| | | |
|---|---|---|
| $VO_2$(B) nanobelts | 274 mAh $g^{-1}$ at 0.1 A $g^{-1}$ | 34 |
| RGO/$VO_2$ composite | 276 mAh $g^{-1}$ at 0.1 A $g^{-1}$ | 35 |
| $H_2V_3O_8$ nanowire | 423.8 mAh $g^{-1}$ at 0.1 A $g^{-1}$ | 12 |
| $V_2O_5$ | 215 mAh $g^{-1}$ at 0.1 A $g^{-1}$ | 10 |
| $H_2V_3O_8$ nanowire/Graphene | 394 mAh $g^{-1}$ at 0.1 A $g^{-1}$ | 36 |
| $V_{10}O_{24}{\cdot}12H_2O$ | 164.5 mAh $g^{-1}$ at 0.2 A $g^{-1}$ after 2 cycles | 37 |
| $V_2O_5{\cdot}nH_2O$/graphene | 381 mAh $g^{-1}$ at 0.3 A $g^{-1}$ | 13 |
| $V_2O_5$ | 470 mAh $g^{-1}$ at 0.2 A $g^{-1}$ | 2 |
| $V_2O_5$ nanofibers | 319 mAh $g^{-1}$ at 0.02 A $g^{-1}$ | 38 |
| $V_6O_{13}{\cdot}nH_2O$ | 395 mAh $g^{-1}$ at 0.1 A $g^{-1}$ | 39 |
| $V_2O_5$ nanospheres | 188.7 mAh $g^{-1}$ at 0.5 A $g^{-1}$ | 40 |
| $V_2O_5$ nanopaper | 375 mAh $g^{-1}$ at 0.5 A $g^{-1}$ | 41 |
| $V_2O_5$ hollow spheres | 280 mAh $g^{-1}$ at 0.2 A $g^{-1}$ | 42 |
| $VS_2$ | 190.3, 136.8 and 121.5 mAh $g^{-1}$ at 0.05, 0.5 and 1 A $g^{-1}$, respectively | 43 |
| $VS_4$@rGO | ~250 mAh $g^{-1}$ at 0.2 A $g^{-1}$ | 44 |

## Table S4

Table S4. Comparison of the electrochemical performance of $NH_4V_3O_8 \cdot 0.5H_2O$ nanowires with the state-of-the-art reported cathode materials towards ARZIBs at 0.1 A $g^{-1}$.c

| **Electrode Materials** | **Electrochemical Performance** | **Ref.** |
|---|---|---|
| **$NH_4V_3O_8 \cdot 0.5H_2O$ nanowires** | **423 mAh $g^{-1}$ at 0.1 A $g^{-1}$** | **This work** |
| $NH_4V_4O_{10}$ | 380.3 mAh $g^{-1}$ at 0.1 A $g^{-1}$ | 4 |
| $(NH_4)_2V_3O_8$ | ~160 mAh $g^{-1}$ at 0.1 A $g^{-1}$ | 4 |
| $NH_4V_3O_8$ | ~80 mAh $g^{-1}$ at 0.1 A $g^{-1}$ | 4 |
| $NH_4V_4O_{10}$ nanobelt | 147 mAh $g^{-1}$ at 0.05 A $g^{-1}$ | 5 |
| $Na_{0.33}V_2O_5$ nanowire | 367.1 mAh $g^{-1}$ at 0.1 A $g^{-1}$ | 29 |
| $Mg_{0.34}V_2O_5 \cdot nH_2O$ | 330 mAh $g^{-1}$ at 0.1 A $g^{-1}$ | 27 |
| $Zn_2(OH)VO_4$ | 204 mAh $g^{-1}$ at 0.1 A $g^{-1}$ | 24 |
| $Fe_5V_{15}O_{39}(OH)_9 \cdot 9H_2O$ | 385 mAh $g^{-1}$ at 0.1A $g^{-1}$ | 9 |
| a-$Zn_3V_2O_7$ | 231 mAh $g^{-1}$ at 0.1A $g^{-1}$ | 16 |
| $VO_2$(B) nanofibers | 357 mAh $g^{-1}$ at 0.1 A $g^{-1}$ | 32 |
| $VO_2$(B) nanobelts | 274 mAh $g^{-1}$ at 0.1 A $g^{-1}$ | 34 |
| RGO/$VO_2$ composite | 276 mAh $g^{-1}$ at 0.1 A $g^{-1}$ | 35 |
| $H_2V_3O_8$ nanowire | 423.8 mAh $g^{-1}$ at 0.1 A $g^{-1}$ | 12 |
| $V_2O_5$ | 215 mAh $g^{-1}$ at 0.1 A $g^{-1}$ | 10 |
| $H_2V_3O_8$ nanowire/Graphene | 394 mAh $g^{-1}$ at 0.1 A $g^{-1}$ | 36 |
| $V_6O_{13} \cdot nH_2O$ | 395 mAh $g^{-1}$ at 0.1 A $g^{-1}$ | 39 |

**References**


1 S.-S. Cao, J.-F. Huang, H.-B. Ouyang, L.-Y. Cao, J.-Y. Li, J.-P. Wu, A simple method to prepare $NH_4V_3O_8$ nanorods as cathode material for Li-ion batteries, *Mater. Lett.*, 2014, **126**, 20-23.

2 N. Zhang, Y. Dong, M. Jia, X. Bian, Y. Wang, M. Qiu, J. Xu, Y. Liu, L. Jiao, F. Cheng, Rechargeable Aqueous Zn–$V_2O_5$ Battery with High Energy Density and Long Cycle Life, *ACS Energy Lett.*, 2018, **3**, 1366-1372.

3 N. Zhang, F. Cheng, Y. Liu, Q. Zhao, K. Lei, C. Chen, X. Liu, J. Chen, Cation-Deficient Spinel $ZnMn_2O_4$ Cathode in $Zn(CF_3SO_3)_2$ Electrolyte for Rechargeable Aqueous Zn-Ion Battery, *J. Am. Chem. Soc.*, 2016, **138**, 12894-12901.

4 H. Li, Z. Liu, G. Liang, Y. Huang, Y. Huang, M. Zhu, Z. Pei, Q. Xue, Z. Tang, Y. Wang, B. Li, C. Zhi, Waterproof and Tailorable Elastic Rechargeable Yarn Zinc Ion Batteries by a Cross-Linked Polyacrylamide Electrolyte, *ACS Nano*, 2018, **12**, 3140-3148.

5 G. Yang, T. Wei, C. Wang, Self-Healing Lamellar Structure Boosts Highly Stable Zinc-Storage Property of Bilayered Vanadium Oxides, *ACS Appl. Mater. Interfaces*, 2018, **10**, 35079-35089.

6 Y. Song, T.-Y. Liu, B. Yao, T.-Y. Kou, D.-Y. Feng, X.-X. Liu, Y. Li, Amorphous Mixed-Valence Vanadium Oxide/Exfoliated Carbon Cloth Structure Shows a Record High Cycling Stability, *Small*, 2017, **13**, 1700067.

7 X. Wang, B. Xi, Z. Feng, W. Chen, H. Li, Y. Jia, J. Feng, Y. Qian, S. Xiong, Layered $(NH_4)_2V_6O_{16}\cdot 1.5H_2O$ nanobelts as a high-performance cathode for aqueous zinc-ion batteries, *J. Mater. Chem. A*, 2019, **7**, 19130-19139.

8 M. H. Alfaruqi, V. Mathew, J. Song, S. Kim, S. Islam, D. T. Pham, J. Jo, S. Kim, J. P. Baboo, Z. Xiu, K.-S. Lee, Y.-K. Sun, J. Kim, Electrochemical Zinc Intercalation in Lithium Vanadium Oxide: A High-Capacity Zinc-Ion Battery Cathode, *Chem. Mater.*, 2017, **29**, 1684-1694.

9 Z. Guo, Y. Ma, X. Dong, J. Huang, Y. Wang, Y. Xia, An Environmentally Friendly and Flexible Aqueous Zinc Battery Using an Organic Cathode, *Angew. Chem.*, 2018, **130**, 11911-11915.

10 P. Hu, M. Yan, T. Zhu, X. Wang, X. Wei, J. Li, L. Zhou, Z. Li, L. Chen, L. Mai, Zn/$V_2O_5$ Aqueous Hybrid-Ion Battery with High Voltage Platform and Long Cycle Life, *ACS Appl. Mater. Interfaces*, 2017, **9**, 42717-42722.

11 G. Wang, X. Lu, Y. Ling, T. Zhai, H. Wang, Y. Tong, Y. Li, LiCl/PVA Gel Electrolyte Stabilizes Vanadium Oxide Nanowire Electrodes for Pseudocapacitors, *ACS Nano*, 2012, **6**, 10296-10302.

12 Y. Zeng, X. Zhang, Y. Meng, M. Yu, J. Yi, Y. Wu, X. Lu, Y. Tong, Achieving Ultrahigh Energy Density and Long Durability in a Flexible Rechargeable Quasi-Solid-State Zn–$MnO_2$ Battery, *Adv. Mater.*, 2017, **29**, 1700274.

13 M. Yan, P. He, Y. Chen, S. Wang, Q. Wei, K. Zhao, X. Xu, Q. An, Y. Shuang, Y. Shao, K. T. Mueller, L. Mai, J. Liu, J. Yang, Water-Lubricated Intercalation in $V_2O_5\cdot nH_2O$ for High-Capacity and High-Rate Aqueous Rechargeable Zinc Batteries, *Adv. Mater.*, 2018, **30**, 1703725.

14 B. Tang, G. Fang, J. Zhou, L. Wang, Y. Lei, C. Wang, T. Lin, Y. Tang, S. Liang, Potassium vanadates with stable structure and fast ion diffusion channel as cathode for rechargeable aqueous zinc-ion batteries, *Nano Energy*, 2018, **51**, 579-587.

15 G. Fang, J. Zhou, Y. Cai, S. Liu, X. Tan, A. Pan, S. Liang, Metal–organic framework-templated two-dimensional hybrid bimetallic metal oxides with enhanced lithium/sodium storage capability, *J. Mater. Chem. A*, 2017, **5**, 13983-13993.

16 B. Sambandam, V. Soundharrajan, S. Kim, M. H. Alfaruqi, J. Jo, S. Kim, V. Mathew, Y.-k. Sun, J. Kim, Aqueous rechargeable Zn-ion batteries: an imperishable and high-energy $Zn_2V_2O_7$

nanowire cathode through intercalation regulation, *J. Mater. Chem. A*, 2018, **6**, 3850-3856.

17 J. Liu, C. Guan, C. Zhou, Z. Fan, Q. Ke, G. Zhang, C. Liu, J. Wang, A Flexible Quasi-Solid-State Nickel–Zinc Battery with High Energy and Power Densities Based on 3D Electrode Design, *Adv. Mater.*, 2016, **28**, 8732-8739.

18 X. Wu, Y. Xiang, Q. Peng, X. Wu, Y. Li, F. Tang, R. Song, Z. Liu, Z. He, X. Wu, Green-low-cost rechargeable aqueous zinc-ion batteries using hollow porous spinel $ZnMn_2O_4$ as the cathode material, *J. Mater. Chem. A*, 2017, **5**, 17990-17997.

19 Y. Cai, F. Liu, Z. Luo, G. Fang, J. Zhou, A. Pan, S. Liang, Pilotaxitic $Na_{1.1}V_3O_{7.9}$ nanoribbons/graphene as high-performance sodium ion battery and aqueous zinc ion battery cathode, *Energy Stor. Mater.*, 2018, **13**, 168-174.

20 N. Zhang, F. Cheng, J. Liu, L. Wang, X. Long, X. Liu, F. Li, J. Chen, Rechargeable aqueous zinc-manganese dioxide batteries with high energy and power densities, *Nat Commun*, 2017, **8**, 405.

21 S. Islam, M. H. Alfaruqi, V. Mathew, J. Song, S. Kim, S. Kim, J. Jo, J. P. Baboo, D. T. Pham, D. Y. Putro, Y.-K. Sun, J. Kim, Facile synthesis and the exploration of the zinc storage mechanism of β-$MnO_2$ nanorods with exposed (101) planes as a novel cathode material for high performance eco-friendly zinc-ion batteries, *J. Mater. Chem. A*, 2017, **5**, 23299-23309.

22 B. Jiang, C. Xu, C. Wu, L. Dong, J. Li, F. Kang, Manganese Sesquioxide as Cathode Material for Multivalent Zinc Ion Battery with High Capacity and Long Cycle Life, *Electrochim. Acta*, 2017, **229**, 422-428.

23 J. Hao, J. Mou, J. Zhang, L. Dong, W. Liu, C. Xu, F. Kang, Electrochemically induced spinel-layered phase transition of $Mn_3O_4$ in high performance neutral aqueous rechargeable zinc battery, *Electrochim. Acta*, 2018, **259**, 170-178.

24 K. Lu, B. Song, Y. Zhang, H. Ma, J. Zhang, Encapsulation of zinc hexacyanoferrate nanocubes with manganese oxide nanosheets for high-performance rechargeable zinc ion batteries, *J. Mater. Chem. A*, 2017, **5**, 23628-23633.

25 M. Yu, Y. Zeng, Y. Han, X. Cheng, W. Zhao, C. Liang, Y. Tong, H. Tang, X. Lu, Valence-Optimized Vanadium Oxide Supercapacitor Electrodes Exhibit Ultrahigh Capacitance and Super-Long Cyclic Durability of 100000 Cycles, *Adv. Funct. Mater.*, 2015, **25**, 3534-3540.

26 D. Kundu, B. D. Adams, V. Duffort, S. H. Vajargah, L. F. Nazar, A high-capacity and long-life aqueous rechargeable zinc battery using a metal oxide intercalation cathode, *Nat. Energy*, 2016, **1**, 16119.

27 F. Ming, H. Liang, Y. Lei, S. Kandambeth, M. Eddaoudi, H. N. Alshareef, Layered $MgxV_2O_5{\cdot}nH_2O$ as Cathode Material for High-Performance Aqueous Zinc Ion Batteries, *ACS Energy Lett.*, 2018, **3**, 2602-2609.

28 C. Xia, J. Guo, P. Li, X. Zhang, H. N. Alshareef, Highly Stable Aqueous Zinc-Ion Storage Using a Layered Calcium Vanadium Oxide Bronze Cathode, *Angew. Chem. Int. Ed.*, 2018, **57**, 3943-3948.

29 P. He, G. Zhang, X. Liao, M. Yan, X. Xu, Q. An, J. Liu, L. Mai, Sodium Ion Stabilized Vanadium Oxide Nanowire Cathode for High-Performance Zinc-Ion Batteries, *Adv. Energy Mater.*, 2018, **8**, 1702463.

30 X. Guo, G. Fang, W. Zhang, J. Zhou, L. Shan, L. Wang, C. Wang, T. Lin, Y. Tang, S. Liang, Mechanistic Insights of $Zn^{2+}$ Storage in Sodium Vanadates, *Adv. Energy Mater.*, 2018, **8**, 1801819.

31 P. Hu, T. Zhu, X. Wang, X. Wei, M. Yan, J. Li, W. Luo, W. Yang, W. Zhang, L. Zhou, Z. Zhou, L.

Mai, Highly Durable $Na_2V_6O_{16}\cdot 1.63H_2O$ Nanowire Cathode for Aqueous Zinc-Ion Battery, *Nano Lett.*, 2018, **18**, 1758-1763.

32 J. Ding, Z. Du, L. Gu, B. Li, L. Wang, S. Wang, Y. Gong, S. Yang, Ultrafast $Zn^{2+}$ Intercalation and Deintercalation in Vanadium Dioxide, *Adv. Mater.*, 2018, **30**, 1800762.

33 J.-S. Park, J. H. Jo, Y. Aniskevich, A. Bakavets, G. Ragoisha, E. Streltsov, J. Kim, S.-T. Myung, Open-Structured Vanadium Dioxide as an Intercalation Host for Zn Ions: Investigation by First-Principles Calculation and Experiments, *Chem. Mater.*, 2018, **30**, 6777-6787.

34 T. Wei, Q. Li, G. Yang, C. Wang, An electrochemically induced bilayered structure facilitates long-life zinc storage of vanadium dioxide, *J. Mater. Chem. A*, 2018, **6**, 8006-8012.

35 A. Sarkar, S. Sarkar, T. Sarkar, P. Kumar, M. D. Bharadwaj, S. Mitra, Rechargeable Sodium-Ion Battery: High-Capacity Ammonium Vanadate Cathode with Enhanced Stability at High Rate, *ACS Appl. Mater. Interfaces*, 2015, **7**, 17044-17053.

36 Q. Pang, C. Sun, Y. Yu, K. Zhao, Z. Zhang, P. M. Voyles, G. Chen, Y. Wei, X. Wang, $H_2V_3O_8$ Nanowire/Graphene Electrodes for Aqueous Rechargeable Zinc Ion Batteries with High Rate Capability and Large Capacity, *Adv. Energy Mater.*, 2018, **8**, 1800144.

37 T. Wei, Q. Li, G. Yang, C. Wang, High-rate and durable aqueous zinc ion battery using dendritic $V_{10}O_{24}\cdot 12H_2O$ cathode material with large interlamellar spacing, *Electrochim. Acta*, 2018, **287**, 60-67.

38 C. Zhou, S. Fan, M. Hu, J. Lu, J. Li, Z.-H. Huang, F. Kang, R. Lv, High areal specific capacity of $Ni_3V_2O_8$/carbon cloth hierarchical structures as flexible anodes for sodium-ion batteries, *J. Mater. Chem. A*, 2017, **5**, 15517-15524.

39 T. Jiao, Q. Yang, S. Wu, Z. Wang, D. Chen, D. Shen, B. Liu, J. Cheng, H. Li, L. Ma, C. Zhi, W. Zhang, Binder-free hierarchical $VS_2$ electrodes for high-performance aqueous Zn ion batteries towards commercial level mass loading, *J. Mater. Chem. A*, 2019, **7**, 16330-16338.

40 P. Liu, R. Lv, Y. He, B. Na, B. Wang, H. Liu, An integrated, flexible aqueous Zn-ion battery with high energy and power densities, *J. Power Sources*, 2019, **410-411**, 137-142.

41 F. Wan, Z. Niu, Design Strategies for Vanadium-based Aqueous Zinc-Ion Batteries, *Angew. Chem. Int. Ed.*, 2019, **0**.

42 C. Wang, D. Fang, H. e. Wang, Y. Cao, W. Xu, X. Liu, Z. Luo, G. Li, M. Jiang, C. Xiong, Uniform Nickel Vanadate ($Ni_3V_2O_8$) Nanowire Arrays Organized by Ultrathin Nanosheets with Enhanced Lithium Storage Properties, *Sci. Rep.*, 2016, **6**, 20826.

43 P. He, M. Yan, G. Zhang, R. Sun, L. Chen, Q. An, L. Mai, Layered $VS_2$ Nanosheet-Based Aqueous Zn Ion Battery Cathode, *Adv. Energy Mater.*, 2017, **7**, 1601920.

44 H. Qin, Z. Yang, L. Chen, X. Chen, L. Wang, A high-rate aqueous rechargeable zinc ion battery based on the $VS_4$@rGO nanocomposite, *J. Mater. Chem. A*, 2018, **6**, 23757-23765.